Frontiers of Information Technology & Electronic Engineering
www.zju.edu.cn/jzus; engineering.cae.cn; www.springerlink.com
ISSN 2095-9184 (print); ISSN 2095-9230 (online)
E-mail: jzus@zju.edu.cn

Optimization design of an interior permanent-magnet synchronous machine for a hybrid hydraulic excavator*

Qi-huai CHEN†1, Qing-feng WANG[1], Tao WANG[2]

([1]*State Key Laboratory of Fluid Power Transmission and Control, Zhejiang University, Hangzhou 310027, China*)

([2]*College of Mechanical and Vehicle Engineering, Hunan University, Changsha 410082, China*)

†E-mail: 11025049@zju.edu.cn

Received Feb. 10, 2015; Revision accepted May 22, 2015; Crosschecked Oct. 10, 2015

Abstract: A hybrid power transmission system (HPTS) is a promising way to save energy in a hydraulic excavator and the electric machine is one of the key components of the system. In this paper, a design process for permanent-magnet synchronous machines (PMSMs) in a hybrid hydraulic excavator (HHE) is presented based on the analysis of the working conditions and requirements of an HHE. A parameterized design approach, which combines the analytical model and the 2D finite element method (FEM), is applied to the electric machine to improve the design efficiency and accuracy. The analytical model is employed to optimize the electric machine efficiency and obtain the stator dimension and flux density distribution. The rotor is designed with the FEM to satisfy the flux requirements obtained in stator design. The rotor configuration of the PMSM employs an interior magnet structure, thus resulting in some inverse saliency, which allows for much higher values in magnetic flux density. To reduce the rotor leakage, a disconnected type silicon steel block structure is adopted. To improve the air gap flux density distribution, the trapezoid permanent magnet (PM) and centrifugal rotor structure are applied to PMSM. Demagnetization and armature reactions are also taken into consideration and calculated by the FEM. A prototype of the newly designed electric machine has been fabricated and tested on the experimental platform. The analytical design results are validated by measurements.

Key words: Analysis, Design, Hybrid hydraulic excavator (HHE), Finite element method (FEM), Interior permanent-magnet (PM) motor, PM synchronous machine (PMSM)

doi:10.1631/FITEE.1500056 **Document code:** A **CLC number:** TM921.41

1 Introduction

Nowadays, people pay much more attention to energy efficiency and environmental protection. As engine emissions are directly related to greenhouse gas emissions, many government agencies and different classification organizations have proposed many stringent standards for fuel consumption and emissions. All these compel us to develop some friendly energy-efficient transmission systems. A hybrid power transmission system (HPTS) is a promising way to substitute for the traditional direct engine drive system, and it has been successfully applied to vehicles (Chan, 2002; Chau *et al.*, 2008; Mutoh, 2012). Research on a hybrid hydraulic excavator (HHE) also has drawn much attention in recent years (Xiao *et al.*, 2008; Wang and Guan, 2013).

The research in the field of electric machines in hybrid, electric vehicle propulsion has been intense over the past few years. However, due to different working conditions of the excavator, the electric machine design for an HHE must be re-considered, and few reports on the development of an electric machine for an HHE can be found. The requirements of an electric machine for HHE applications include high torque density, high power density, quick response, and high efficiency. According to the electric

* Project supported by the National Natural Science Foundation of China (Nos. 51475414 and 51221004)

ORCID: Qi-huai CHEN, http://orcid.org/0000-0003-1496-1366

machines used in hybrid, electric vehicles (Zhu and Howe, 2007; El-Refaie, 2010; Laskaris and Kladas, 2010; Dorrel *et al.*, 2011; Phi *et al.*, 2011; Wang *et al.*, 2011; Pellegrino *et al.*, 2012a; Reddy *et al.*, 2012; Sizov *et al.*, 2012; Morimoto *et al.*, 2014; Nerg *et al.*, 2014), the most popular electric machine type for traction applications is the permanent-magnet synchronous machine (PMSM). Its efficiency and torque density are the highest among the present-day electrical machines (Nerg *et al.*, 2014). Moreover, due to the inverse saliency of the interior magnet PMSM, some additional benefits can be achieved. For an HHE, the PMSM is also an ideal candidate.

An HHE power transmission system involves some special working conditions, including uncontrollable and severe volatility mechanical torque input, variable DC voltage output, and constant speed rotation. Therefore, the design process of the electric machine in an HHE differs from that of an electric machine in hybrid, electric vehicles, where the load is smoother than an HHE and the machine is designed for a wide speed range.

The PMSM design methodology has been widely discussed in the literature. A direct method is to build the governing equation for magnetic scalar potential and obtain the flux density distribution (Markovic and Perriard, 2009; Zhu *et al.*, 2010). Another approach is to use a magnetic equivalent circuit to design the electric machine (Vaez-Zadeh and Ghasemi, 2005; Cassimere *et al.*, 2009; Alberti *et al.*, 2010). In the above two methods, researchers always assumed that the permeability of iron is infinite. However, in fact, the nonlinear impact of iron saturation will affect the design results. Taking the nonlinearity of the magnetic circuit into account, Comanescu *et al.* (2003) used spline interpolation to capture the characteristics of iron magnetization. Bianchi *et al.* (2006) demonstrated some useful design criteria for high efficiency PM machines by using the analytical method. The finite element method (FEM), a well-known design tool, can obtain accurate results (El-Refaie *et al.*, 2006; Alberti *et al.*, 2011; Eriksson and Bernhoff, 2011; Pellegrino *et al.*, 2012b; Kim *et al.*, 2014). However, FEM usually consumes a lot of time to obtain the results. So, it is often regarded as an auxiliary method to validate analytical results. Wang and Wang (2012) expounded an efficient method which combines the analytical model and FEM to design the PMSM.

This paper presents a complete design process of the PMSM for HHE applications. A feasible PMSM structure for an HHE is proposed. First, the HHE power transmission system is analyzed and preliminary design of an electric machine is carried out. Second, the stator is designed by using an analytical model to optimize the dimension and field distribution. Third, the rotor is designed with the FEM to obtain the pre-assumed field distribution. Fourth, the armature reactions and demagnetizations are validated. Finally, a prototype of an electric machine is fabricated and tested on an experimental platform of the HHE power transmission system.

2 Specific conditions and preliminary consideration

Before PMSM design, we should investigate the specification of the PMSM in an HHE. In a traditional excavator (Fig. 1a), the engine directly drives the hydraulic pump. The engine throttle is preset and fixed. The oil flow rate in the hydraulic system is controlled by the displacement of the pump. Due to the severe fluctuation of the load, the efficiency of the engine is low. In the HHE indicated in Fig. 1b, the engine, PMSM, and pump are coaxially connected.

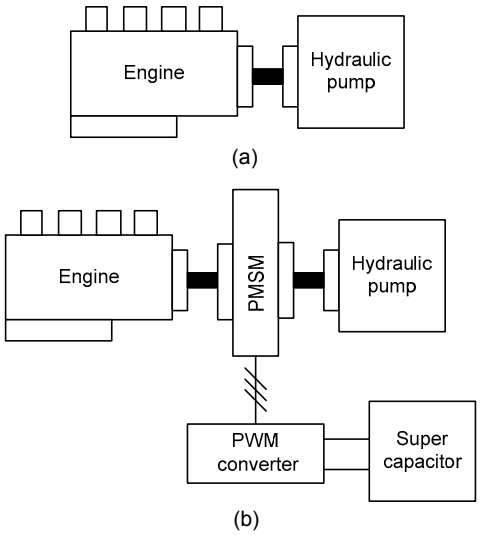

Fig. 1 Power transmission system
(a) Traditional excavator; (b) Hybrid hydraulic excavator

The PMSM assists the engine in driving the pump, which keeps the engine to work in a high efficiency range. However, the PMSM is not only a machine to drive the hydraulic pump, but also a velocity adjuster of the engine. Moreover, the electric power consumed or produced by the PMSM should be controlled to allow the state of charge (SOC) of the super capacitor to operate in a required range.

The mechanical torque absorbed by the hydraulic pump is uncontrollable and varies with the load. Fig. 2a gives the normalized load profile of a hydraulic pump in five typical working cycles. The load of the pump changes severely and is distributed in a wide range. The mechanical torque produced by the PMSM can be obtained by optimizing the HPTS according to the load profile of the pump. Through optimizing the HPTS for an HHE, the fuel consumption decreases by about 8%. Because the HPTS optimizations have no relationship with PMSM design, we do not introduce them in detail. The normalized mechanical torque produced by a PMSM in an HHE is shown in Fig. 2b. We can see that the PMSM torque fluctuates severely as well. Fig. 3 gives the mechanical characteristics of the PMSM in an HHE. When the pump torque is greater than the engine torque, the PMSM works as a motor; when the pump torque is smaller than the engine torque, it works as a generator. Furthermore, due to the use of the PMSM, the rotation speed of HPTS operates in a small range.

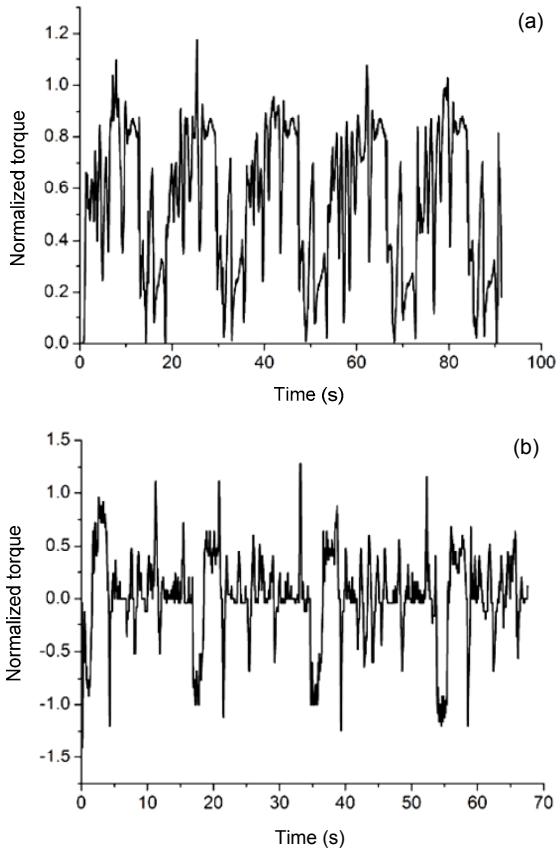

Fig. 2 Normalized mechanical torque
(a) Hydraulic pump; (b) PMSM

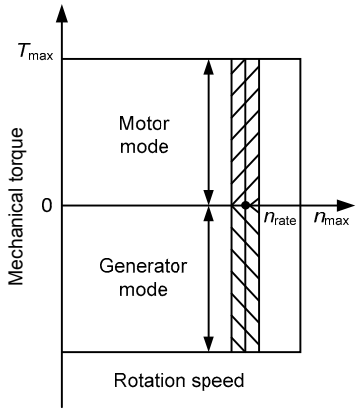

Fig. 3 PMSM mechanical characteristics

In this study, the parameters of the PMSM are given as follows: the rating torque is 200 N·m, the rating rotation speed 1800 r/min, the rating power 38 kW, and the DC voltage of the super capacitor 280–380 V.

In machine design, a rotor construction, in which the interior NdFeB magnet structure is employed, is selected as a base solution. There are two practical reasons for this selection. First, the structure involves more important magnetic loading (Laskaris and Kladas, 2010) and the rotor leakage can be reduced by adopting the disconnected type silicon steel block structure. Second, the structure uses not only the magnet torque but also the reluctance torque, which occurs because of the difference between the two axes inductances. Furthermore, to improve the air gap flux density distribution, the trapezoid PM and centrifugal rotor structure are applied to the PMSM. The structure of the PMSM rotor is shown in Fig. 4.

As aforementioned, the rotation speed of the PMSM operates in a small range, so the iron loss is primarily decided by the quality of the stator. To make the stator structure light, a high pole number is an ideal solution, as the number of flux paths for the

main flux linearly increases with the increase of the pole number. However, a high pole number, which leads to the increase of the winding end, will increase the copper loss. So, the number of pole pairs is chosen to be three. To reduce torque ripples, the one-slot skew and distributed windings are used. The slot number is 36, because a small slot pitch is beneficial to the manufacture of the skew slots.

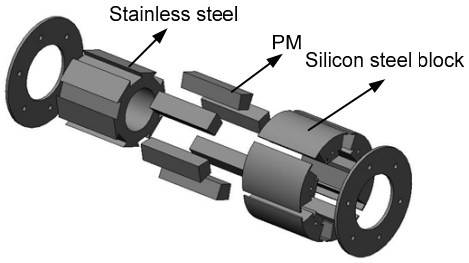

Fig. 4 Structure of the PMSM rotor

In addition to the above preliminary consideration, the PMSM in an HHE is restricted by many other factors, such as efficiency, the dimension constraint, manufacture, control performance, and irreversible demagnetization. In the design process, these factors should be taken into consideration as much as possible.

3 Stator design

A PMSM design is a complicated multi-object optimization problem. The FEM is an accurate method, but it requires a lot of time. In this study, we use an analytical model to optimize the stator and obtain the target geometry and flux density distribution of the stator. The goal of the optimization is to achieve high efficiency in the PMSM. The efficiency of the PMSM is decided primarily by iron loss and copper loss. Meanwhile, iron loss and copper loss are related to the dimension and flux density distribution of the stator.

3.1 Analysis based on model

Fig. 5 shows the vector presentation of the PMSM. $\boldsymbol{E}_\mathrm{s}$ is the back electromotive force (EMF), $\boldsymbol{i}_\mathrm{s}$ the stator current vector, $\boldsymbol{u}_\mathrm{s}$ the stator voltage vector, $\boldsymbol{\psi}_\mathrm{pm}$ the flux linkage vector caused by PM, $\boldsymbol{\psi}_\mathrm{s}$ the stator flux linkage vector, L_d the direct-axis inductance, L_q the quadrature-axis inductance, $\boldsymbol{i}_d$ the direct-axis current vector, $\boldsymbol{i}_q$ the quadrature-axis current vector, and β the phase angle.

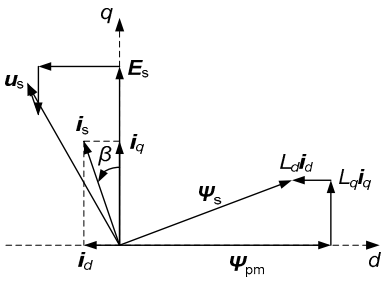

Fig. 5 Vector presentation of the PMSM

The steady stator voltage can be written as

$$u_\mathrm{s}=\sqrt{(R_\mathrm{a}i_d-w_\mathrm{e}L_qi_q)^2+(R_\mathrm{a}i_q+w_\mathrm{e}L_di_d+E_\mathrm{s})^2}, \quad (1)$$

where R_a is the winding resistance and w_e the electrical angular speed. For star-connected winding, the amplitude of stator voltage (u_s) and DC bus voltage (U_dc) should satisfy the following inequality:

$$u_\mathrm{s}\le\frac{U_\mathrm{dc}}{\sqrt{3}}. \quad (2)$$

As can be seen from Eq. (1) and inequality (2), the back EMF is restricted by the DC voltage as mentioned above, varying from 280 V to 380 V. To ensure the reliable operation of the PMSM, the back EMF at the rating speed is chosen by

$$E_\mathrm{s}=\frac{k_\mathrm{e}U_\mathrm{dc\,min}}{\sqrt{3}}, \quad (3)$$

where k_e is the safe coefficient and $U_\mathrm{dc\,min}$ the minimum DC voltage. The PM flux linkage can be obtained according to the following expression:

$$E_\mathrm{s}=w_\mathrm{e}\Psi_\mathrm{pm}. \quad (4)$$

The rating current can be acquired according to the torque expression. The torque of the PMSM can be given as

$$T=\frac{3}{2}p\left(\psi_\mathrm{pm}i_\mathrm{s}\cos\beta+\frac{1}{2}(L_d-L_q)i_\mathrm{s}^2\sin(2\beta)\right), \quad (5)$$

where p is the number of pole pairs. In Eq. (5), the torque can be divided into two parts. One part is the electro-magnetic torque caused by the interaction between rotor and stator flux:

$$T_{\mathrm{e}}=\frac{3}{2}p\psi_{\mathrm{pm}}i_{\mathrm{s}}\cos\beta. \tag{6}$$

The other part is the reluctance torque caused by the inverse saliency:

$$T_{\mathrm{rel}}=\frac{3}{4}p(L_d-L_q)i_{\mathrm{s}}^2\sin(2\beta). \tag{7}$$

As aforementioned, the mechanical torque absorbed by the pump changes severely. The PMSM, which assists the engine in driving the pump and keeps the engine to operate in a high efficiency area, should satisfy the fast response requirement. This implies that the time constant of the PMSM should be small. The time constant is decided by the resistance and inductance. To reduce the time constant and guarantee the efficiency of the PMSM, the inductance of the PMSM should be small. Therefore, the designed PMSM in this article can produce the reluctance torque, but it only slightly affects the rating current. When designing the stator of the PMSM, we ignore the influence of reluctance torque and use a zero d-axis current control. The rating current can be obtained according to the rewritten torque expression:

$$T=\frac{3}{2}p\psi_{\mathrm{pm}}i_{\mathrm{s}}. \tag{8}$$

Because of the anisotropic nature of the magnetic material, the axial end has little effect on the calculation of the PM flux linkage. ψ_{pm} can be calculated as

$$\psi_{\mathrm{pm}}=\frac{2}{\pi}k_{\mathrm{w}}N_{\mathrm{p}}B_{\mathrm{g}}\tau L_{\mathrm{i}}, \tag{9}$$

where k_{w} is the winding factor, N_{p} the number of coils per phase, B_{g} the amplitude of the air gap flux density, τ the pole pitch, and L_{i} the PM axial length. The pole pitch can be expressed as

$$\tau=\frac{\pi D_{\mathrm{i}}}{2p}, \tag{10}$$

where D_{i} is the inner diameter of the stator. According to Eqs. (9) and (10), the number of coils per phase can be derived as

$$N_{\mathrm{p}}=\frac{p\psi_{\mathrm{pm}}}{k_{\mathrm{w}}B_{\mathrm{g}}L_{\mathrm{i}}D_{\mathrm{i}}}. \tag{11}$$

The simplified cross section of the PMSM stator is shown in Fig. 6, where D_{o} is the outer diameter of the stator, h_{j2} the yoke height, h_{t2} the tooth width, t_2 the tooth pitch, and h_{02}, h_2, b_{02}, d_2, and r_2 the basic sizes of the pear-shaped slot. The tooth width (h_{t2}), tooth pitch (t_2), and yoke height (h_{j2}) can be respectively expressed as

$$h_{\mathrm{t2}}=\frac{B_{\mathrm{g}}t_2}{k_{\mathrm{Fe}}B_{\mathrm{t2}}}, \tag{12}$$

$$t_2=\frac{\pi D_{\mathrm{i}}}{Q}, \tag{13}$$

$$h_{\mathrm{j2}}=\frac{D_{\mathrm{i}}B_{\mathrm{g}}}{2k_{\mathrm{Fe}}pB_{\mathrm{j2}}}, \tag{14}$$

where k_{Fe} is the stacking factor, B_{t2} the flux density in the stator tooth, Q the number of slots, and B_{j2} the flux density of the stator yoke. According to Eqs. (12)–(14), the flux densities in B_{t2} and B_{j2} can be obtained. For single-layer winding, the slot area can be acquired according to the geometry shown in Fig. 6:

$$\begin{aligned}S=&\frac{2r_2+d_2}{2}\cdot\left(\frac{D_{\mathrm{o}}-D_{\mathrm{i}}}{2}-h_{\mathrm{j2}}-r_2-h_2-h_{02}\right)\\&+\frac{\pi r_2^2}{2}+\frac{(d_2+b_{02})h_2}{2}.\end{aligned} \tag{15}$$

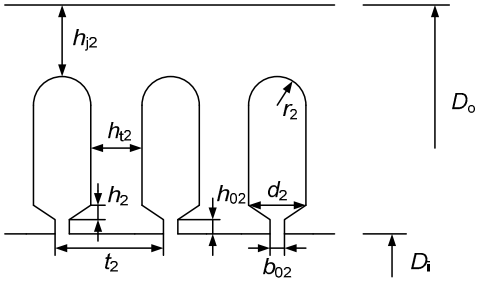

Fig. 6 Simplified cross section of the PMSM stator

The full factor of slot can be written as

$$k_{\mathrm{f}}=\frac{6S_{\mathrm{c}}N_{\mathrm{p}}}{SQ}, \tag{16}$$

where S_{c} is the cross-sectional area of the conductor, and it can be obtained as

$$S_{\mathrm{c}}=\frac{i_{\mathrm{s}}}{\sqrt{2}J}, \tag{17}$$

where J is the current density. According to Eqs. (15)–(17), the outer diameter of the PMSM stator can be calculated. The winding resistance can be given as

$$R_{\mathrm{a}}=\rho_{\mathrm{c}}N_{\mathrm{p}}\frac{L_{\mathrm{t}}}{S_{\mathrm{c}}}, \tag{18}$$

where ρ_{c} is the copper resistivity and L_{t} the total length of a coil. The stator coil geometry is illustrated in Fig. 7. L_{t} can be given as

$$L_{\mathrm{t}}=l_{\mathrm{i}}+2(d+l_{\mathrm{ES}}), \tag{19}$$

where d is decided by the manufacture and l_{ES} can be calculated according to Fig. 6:

$$\begin{cases} l_{\mathrm{ES}}=k_{\mathrm{c}}\tau_{\mathrm{c}}, \\ \tau_{\mathrm{c}}=\dfrac{\pi[D_{\mathrm{i}}+2(h_{02}+h_2)+h_{\mathrm{j2}}+r_2]}{2p}, \end{cases} \tag{20}$$

where k_{c} is the empirical coefficient. From Eq. (18), the copper loss can be given as

$$P_{\mathrm{cu}}=\frac{3}{2}i_{\mathrm{s}}^2R_{\mathrm{a}}. \tag{21}$$

The iron loss per unit volume can be calculated as (Boglietti *et al.*, 2003; Eriksson and Bernhoff, 2011)

$$P_{\mathrm{i}}'=k_{\mathrm{h}}fB^2+k_{\mathrm{ex}}f^{1.5}B^{1.5}+k_{\mathrm{ed}}f^2B^2, \tag{22}$$

where k_{h} is the hysteresis loss coefficient, k_{ex} the excess loss coefficient, k_{ed} the eddy current loss coefficient, B the flux density in iron, and f the frequency. The iron losses of the stator tooth P_{it} and yoke P_{iy} can be given as

$$\begin{cases} P_{\mathrm{it}}=k_{\mathrm{Fe}}P_{\mathrm{i}}'V_{\mathrm{t}}\big|_{B=B_{\mathrm{t2}}}, \\ P_{\mathrm{iy}}=k_{\mathrm{Fe}}P_{\mathrm{i}}'V_{\mathrm{y}}\big|_{B=B_{\mathrm{j2}}}, \end{cases} \tag{23}$$

where V_{t} is the volume of the tooth and V_{y} the volume of the yoke. The total loss can be expressed as

$$P_{\mathrm{t}}=P_{\mathrm{cu}}+P_{\mathrm{it}}+P_{\mathrm{iy}}. \tag{24}$$

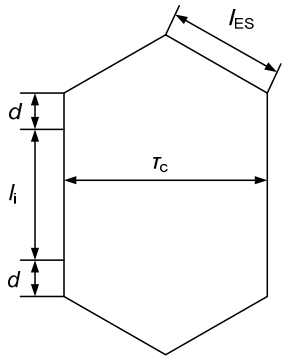

Fig. 7 Schematic diagram of a stator coil

3.2 Efficiency optimization

Based on the analytical model discussed above, the relationship between stator geometry and flux density distribution has been illustrated. In this part, optimization is implemented to design the stator. The optimization target is to improve PMSM efficiency, and thus we use the minimum total loss as the objective function. The variables including D_{i}, L_{i}, b_{t2}, h_{j2}, and B_{g} are chosen to be optimized. The outer diameter (D_{o}) is constrained by the installation space. The flux densities B_{t2} and B_{j2} are also considered as constraint conditions. Therefore, the PMSM stator optimization problem can be expressed as follows:

$$\begin{aligned} &\min P_{\mathrm{t}}(D_{\mathrm{i}},L_{\mathrm{i}},b_{\mathrm{t2}},h_{\mathrm{j2}},B_{\mathrm{g}}) \\ &\text{s.t.}\begin{cases} f(D_{\mathrm{i}},L_{\mathrm{i}},b_{\mathrm{t2}},h_{\mathrm{j2}},B_{\mathrm{g}})\le f_{\max}, f=D_{\mathrm{o}},B_{\mathrm{t2}},B_{\mathrm{j2}}, \\ x_{\min}\le x\le x_{\max}, x=D_{\mathrm{i}},L_{\mathrm{i}},b_{\mathrm{t2}},h_{\mathrm{j2}},B_{\mathrm{g}}. \end{cases} \end{aligned} \tag{25}$$

Particle swarm optimization (PSO) is employed to explore the optimization problem. PSO is a population-based stochastic optimization method, and it has the advantages of convenient realization, simple rules, and promising optimization ability to address

various problems. It searches for the optimal solution from a population of particles with velocities, each of which represents a feasible solution. In the iterative optimization procedure, every particle keeps tracking its individual best position and is associated with the fest fitness. The inequality constraints are taken into consideration by using a penalty function. The iteration is performed until a sufficiently good result is achieved or the maximum number of iterations has been reached.

In PSO, the initial values of variables are random. The number of particles and the maximum number of iterations selected in this study are 40 and 1000, respectively. The main parameters of the PMSM stator after optimization are given in Table 1. The total loss varying with the number of iterations in the optimization is shown in Fig. 8. As can be seen, the optimized total loss is significantly reduced.

Table 1 Main parameters of the PMSM stator

Parameter	Value
Number of pole pairs	3
Number of phases	3
Number of stator slots	36
Outer diameter	260 mm
Inner diameter	180 mm
Axial iron length	115 mm
Tooth width	10 mm
Yoke height	20.75 mm
Air gap flux density	1.15 T
Tooth flux density	1.9 T
Yoke flux density	1.75 T
Winding connection	Star
Total loss	2283.768 W

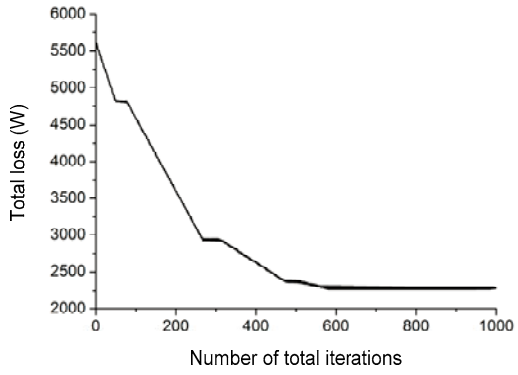

Fig. 8 Total loss varying with the iteration number

4 Rotor design

In this section, FEM is used to design the rotor structure and obtain an air gap flux density, which is a fundamental component with the predesigned value in Section 3 and a relatively small harmonic distortion. The schematic of one pole of the designed PMSM is shown in Fig. 9. It can be seen that the air gap length increases with the increase of the angle (θ). In the d-axis direction, the air gap length is the smallest. We define a centrifugal ratio, which can be expressed as

$$c_r=r_1/r_2, \tag{26}$$

where r_1 and r_2 are the actual and maximum radii of the rotor, respectively.

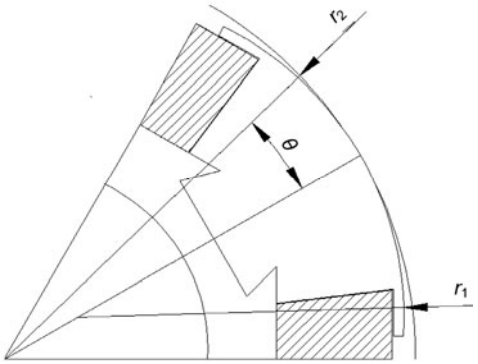

Fig. 9 Schematic of one pole of the designed PMSM

There are two reasons for this design structure. First, as we know, the length of the air gap is primarily affected by the manufacture. Meanwhile, the length of the air gap affects the usage of the PM. The shorter the air gap, the less usage of the PM, but the more prone to irreversible demagnetization the PM. This structure can realize the target air gap flux density and reduce the usage of PM, and at the same time, ensure no irreversible demagnetization. Second, the structure can reduce the effects of the high-order harmonic. To investigate the fundamental component and the harmonic distortion of the PMSM, a series expansion of the air gap flux density is performed. The harmonic distortion can be calculated as

$$H_d=\frac{1}{B_1}\sqrt{\sum_{i=2}^{\infty}B_i}, \tag{27}$$

where B_i ($i\in\mathbb{Z}$) is the ith-order harmonic component and B_1 the fundamental component.

For convenient manufacture and to reduce the usage of the PM, the shortest length of the air gap is chosen as 1 mm. The air gap flux density is primarily decided by five parameters, including the centrifugal ratio, the magnetic isolation groove length, the topline length of the PM, the baseline length of the PM, and the height of the PM. It should be noted that it is difficult to design and optimize the rotor structure of the PMSM.

To simplify the design of the PMSM, we neglect the influence of the magnetic isolation groove. A fixed length of groove length is given to ensure the effective magnetic separation. First, a constant centrifugal ratio c_r=1 and cuboid PM are applied to investigate the fundamental component of the air gap flux density and the harmonic distortion, and also to analyze the geometry of the PM. Figs. 10 and 11 illustrate that both the fundamental component and harmonic distortion of the air gap flux density vary with the PM dimension.

In this circumstance, the irreversible demagnetization will take place or/and the harmonic distortion will be relatively large. From Figs. 10 and 11, we can find that the height of the PM has significant influence on the fundamental component of the air gap flux density and harmonic distortion. So, a high PM is an ideal candidate for the PMSM rotor.

To ensure no irreversible demagnetization and reduce the harmonic distortion, the structure in Fig. 9 is applied. The centrifugal ratio is important, because a small centrifugal ratio will not only reduce the height of the PM but also increase the usage of the PM. A large centrifugal ratio will cause irreversible demagnetization or/and relatively large harmonic distortion.

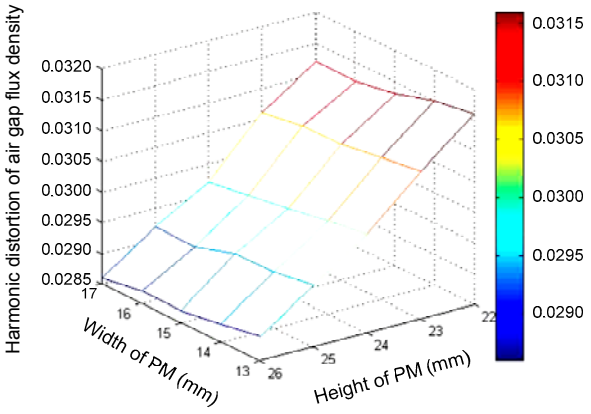

Fig. 11 Harmonic distortion of the air gap flux density varying with the PM dimension (c_r=1)

As aforementioned, a high PM is an ideal candidate for the designed PMSM. Therefore, the height of the PM depends on the centrifugal ratio on the foundation for creating enough mechanical strength. By using FEM, a series of centrifugal ratios are tested and the optimized centrifugal ratio is c_r=0.8. The height of the PM is 25 mm. To further determine the optimization of the harmonic distortion, the lengths of the topline and baseline of the PM are analyzed. Figs. 12 and 13 show that both the fundamental component and harmonic distortion of the air gap flux density vary with the PM dimension.

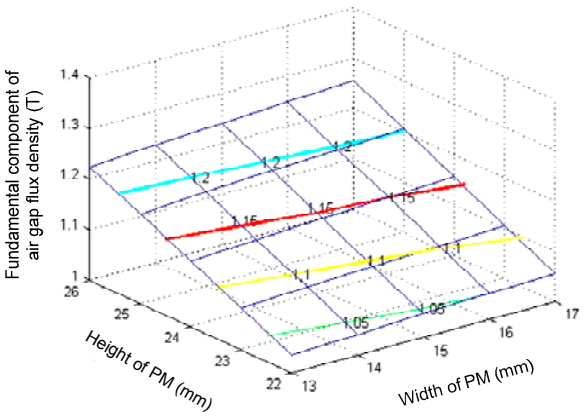

Fig. 10 Fundamental component of the air gap flux density varying with the PM dimension (c_r=1)

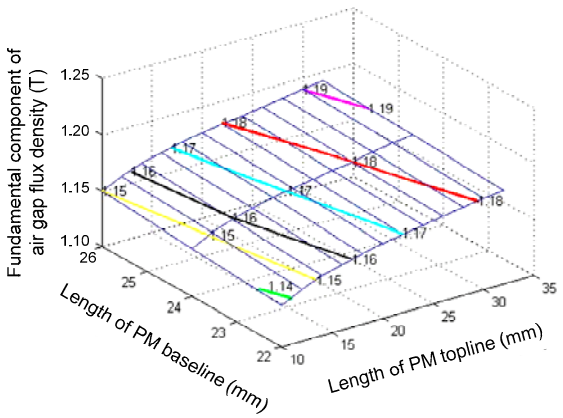

Fig. 12 Fundamental component of the air gap flux density varying with the PM dimension (c_r=0.8)

According to the stator design in Section 3, the predesigned value of the fundamental component of the air gap flux density is 1.15 T. However, considering the manufacture, in which the air gap will be produced in the process of PM installation, the optimized results we have chosen are: the topline length of the PM is 30 mm, the baseline length of the PM 24 mm, the height of the PM 25 mm, and the centrifugal ratio of the rotor 0.8. The corresponding air gap flux density is 1.18 T and the harmonic distortion is 0.0285.

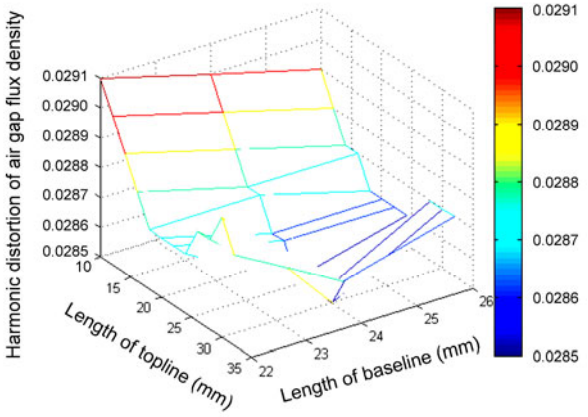

Fig. 13 Harmonic distortion of the air gap flux density varying with the PM dimension (c_r=0.8)

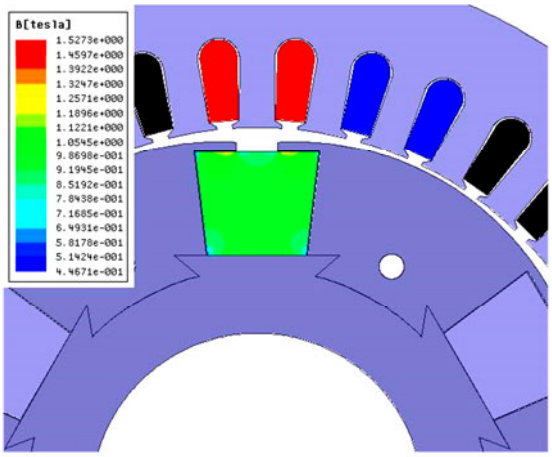

Fig. 14 PM flux density in the PMSM under the maximum demagnetization

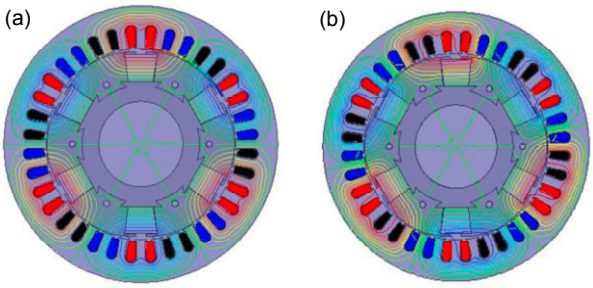

Fig. 15 Flux distribution without load (a) and at full load (b)

5 Demagnetization and armature reaction

To validate PM demagnetization, the PMSM under the maximum demagnetization condition is tested using FEM. The demagnetized load angle is 180°, the magnitude of the current is 200 A, and the PM temperature is 100 °C. The air gap produced in the process of manufacture is also taken into consideration. We assume that the unilateral air gap length of the PM is 0.2 mm. The flux density of the PMSM is given in Fig. 14. As can be seen, the minimum flux density of the PM is about 0.45 T, which is above the knee point of the PM.

To evaluate the effect of armature reaction, the flux distributions calculated using FEM without load and at full load are shown in Fig. 15. The maximum flux density in the stator tooth is 1.7 T without load and 1.9 T at full load. The maximum flux density in the stator yoke is 1.5 T without load and 1.8 T at full load.

6 Prototype and experiment

According to the above design results, a prototype PMSM has been fabricated. The stator and rotor of the PMSM are shown in Fig. 16. The stator and rotor are manufactured according to the above analyses. To test the performance of the PMSM, a test platform has been built. Fig. 17 shows the experimental platform of the HHE power transmission

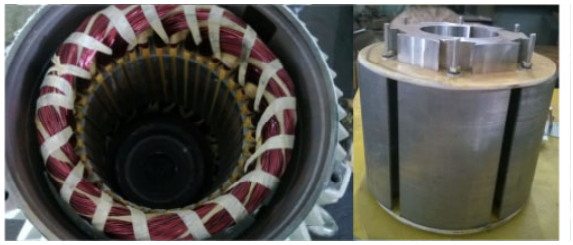

Fig. 16 Fabricated PMSM
(a) Stator; (b) Rotor

Fig. 17 Experimental platform of the HHE power transmission system

system. As can be seen, the engine, PMSM, and pump are coaxially connected. The engine output torque and pump input torque are measured by two torque transducers. The electric power consumed or produced by the PMSM is stored in a super capacitor with a capacity of 37 F.

The PMSM is controlled by a DS1104 digital signal processing card (dSpace GmbH, Germany), in which the control strategies are executed. The PMSM phase current and super capacitor DC current and DC voltage are measured by using Hall sensors and a voltage sensor. The displacement of the PMSM is measured by an encoder and its output is connected to the DS1104's encoder interface. Other outputs of the sensors are connected to the analog-to-digital (AD) interfaces of DS1104.

First, the back EMF without load is tested. The back EMF waveform of the PMSM without load and at about 1800 r/min is shown in Fig. 18. As can be seen, the waveform is very close to a sinusoidal waveform. Meanwhile, the cogging torque is very small.

Then the torque outputs at different currents are tested. We use a zero *d*-axis current control and the maximum torque control to obtain the PMSM toque output at different currents, respectively. Fig. 19 shows the comparison between the experiments and analytical torque, in which the PMSM works as a motor. The analytical torque is calculated using a zero *d*-axis control. Because the inductance of the designed PMSM in this article is small, the difference between the torques obtained using a maximum torque control and zero *d*-axis current control at the same current is small. It verifies the rationality of the stator design in which the zero *d*-axis current control is used to obtain the rating current. However, due to the inverse saliency, the efficiency of the PMSM can be further improved to some extent.

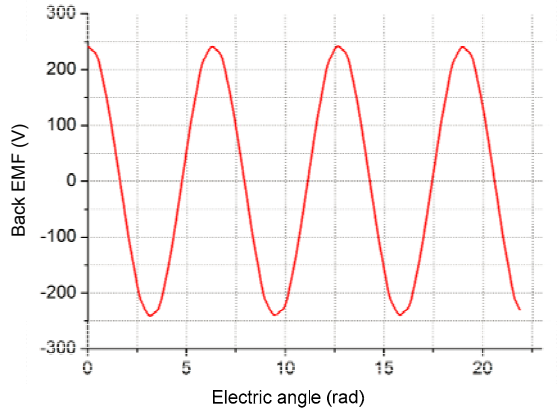

Fig. 18 Back EMF of PMSM

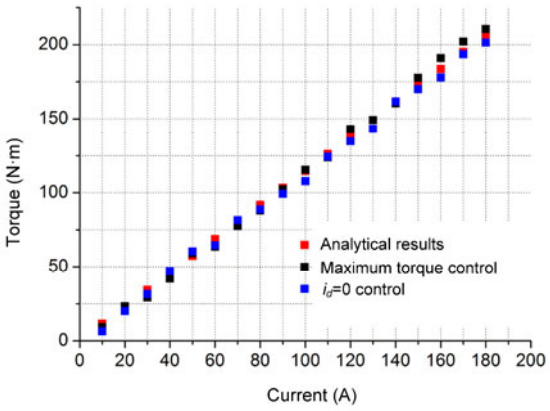

Fig. 19 PMSM torque output at different currents

The efficiency of the PMSM is also measured. Fig. 20 shows the efficiency of the PMSM at various working points and rating rotation speeds. As can be observed, the efficiency of the PMSM is above 90% in the large range. The copper loss is determined by measuring the stator phase resistance and the respective loading current. The total loss is calculated according to the output power of the PMSM and power consumed by the super capacitor. Fig. 21 shows the comparison between the copper loss and

total loss at about 1800 r/min and at different loading currents. The total loss is composed of copper loss, iron loss, mechanical loss, conductor loss, and rectifier loss. As can be seen from Fig. 21, due to the special working condition of the HHE and the loss of the PMSM which is caused by iron loss, mechanical loss, conductor loss, and rectifier loss, the changes are small under different loading currents and are decided mainly by iron loss.

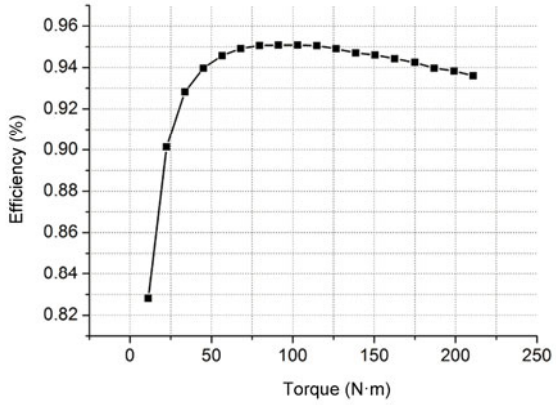

Fig. 20 Efficiency of the PMSM

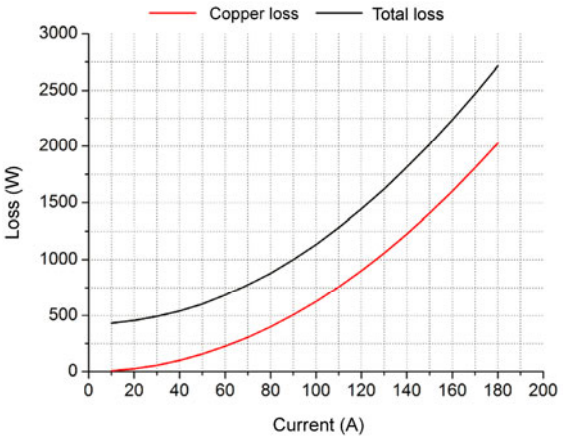

Fig. 21 Copper loss and total loss at different loading currents

Table 2 shows the comparison between the analytical and measured parameters at different rating points. It can be seen that the measured flux linkage and resistance are in accord with the analytical values. However, the measured efficiency of the PMSM is lower than the analytical efficiency, even though the maximum torque control is applied. This is because when calculating the analytical efficiency the influence of the mechanical and rectifier losses is neglected.

Table 2 Comparison between the analytical and measured parameters

Parameter	Value	
	Analytical	Measured
Flux linkage (V·s)	0.255	0.249
Resistance (Ω)	0.0431	0.0417
Efficiency (%)	93.99	93.67

7 Conclusions

This paper introduces the design procedure of a PMSM for HHE applications. The design is based on the analysis of the requirements and working conditions of an HHE. We use an analytical model to design the stator of the PMSM, and FEM to design the rotor. The rotor uses an interior NdFeB magnet structure to involve more important magnetic loading. The disconnected-type silicon steel block structure is applied to reduce the rotor leakage. Furthermore, the trapezoid PM and centrifugal rotor structure are used to improve the air gap flux density distribution. The design of the PMSM has been validated by the experimental results. The PMSM is intended to be incorporated in a 20 t HHE.

References

Alberti, L., Barcaro, M., Pré, M.D., *et al*., 2010. IPM machine drive design and tests for an integrated starter-alternator application. *IEEE Trans. Ind. Appl*., **46**(3):993-1001. [doi:10.1109/TIA.2010.2045323]

Alberti, L., Bianchi, N., Bolognani, S., 2011. Variable-speed induction machine performance computed using finite-element. *IEEE Trans. Ind. Appl.*, **47**(2):789-797. [doi:10.1109/TIA.2010.2103914]

Bianchi, N., Bolognani, S., Frare, P., 2006. Design criteria for high-efficiency SPM synchronous motors. *IEEE Trans. Energy Conv*., **21**(2):396-404. [doi:10.1109/TEC.2005.853720]

Boglietti, A., Cavagnino, A., Lazzari, M., *et al*., 2003. Predicting iron losses in soft magnetic materials with arbitrary voltage supply: an engineering approach. *IEEE Trans. Magn.*, **39**(2):981-989. [doi:10.1109/TMAG.2003.808599]

Cassimere, B.N., Sudhoff, S.D., Sudhoff, D.H., 2009. Analytical design model for surface-mounted permanent-magnet synchronous machines. *IEEE Trans. Energy Conv*., **24**(2):347-357. [doi:10.1109/TEC.2009.2016139]

Chan, C.C., 2002. The state of the art of electric and hybrid vehicles. *Proc. IEEE*, **90**(2):247-275. [doi:10.1109/5.989873]

Chau, K.T., Chan, C.C., Liu, C., 2008. Overview of permanent-magnet brushless drives for electric and hybrid electric vehicles. *IEEE Trans. Ind. Electron.*, **55**(6):2246-2257. [doi:10.1109/TIE.2008.918403]

Comanescu, M., Keyhani, A., Dai, M., 2003. Design and analysis of 42-V permanent-magnet generator for automotive applications. *IEEE Trans. Energy Conv.*, **18**(1): 107-112. [doi:10.1109/TEC.2002.808380]

Dorrel, D.G., Knight, A.M., Popescu, M., 2011. Performance improvement in high-performance brushless rare-earth magnet motors for hybrid vehicles by use of high flux-density steel. *IEEE Trans. Magn.*, **47**(10):3016-3019. [doi:10.1109/TMAG.2011.2157103]

El-Refaie, A.M., 2010. Fractional-slot concentrated-windings synchronous permanent magnet machines: opportunities and challenges. *IEEE Trans. Ind. Electron.*, **57**(1): 107-121. [doi:10.1109/TIE.2009.2030211]

El-Refaie, A., Jahns, T.M., McCleer, P.J., *et al.*, 2006. Experimental verification of optimal flux weakening in surface PM machines using concentrated windings. *IEEE Trans. Ind. Appl.*, **42**(2):443-453. [doi:10.1109/TIA.2006.870043]

Eriksson, S., Bernhoff, H., 2011. Loss evaluation and design optimisation for direct driven permanent magnet synchronous generators for wind power. *Appl. Energy*, **88**(1):265-271. [doi:10.1016/j.apenergy.2010.06.010]

Kim, S., Park, S., Park, T., *et al.*, 2014. Investigation and experimental verification of a novel spoke-type ferrite-magnet motor for electric-vehicle traction drive applications. *IEEE Trans. Ind. Electron.*, **61**(10):5763-5770. [doi:10.1109/TIE.2014.2304697]

Laskaris, K.I., Kladas, A.G., 2010. Internal permanent magnet motor design for electric vehicle drive. *IEEE Trans. Ind. Electron.*, **57**(1):138-145. [doi:10.1109/TIE.2009.2033086]

Markovic, M., Perriard, Y., 2009. Optimization design of a segmented Halbach permanent-magnet motor using an analytical model. *IEEE Trans. Magn.*, **45**(7):2955-2960. [doi:10.1109/TMAG.2009.2015571]

Morimoto, S., Ooi, S., Inoue, Y., *et al.*, 2014. Experimental evaluation of a rare-earth-free PMASynRM with ferrite magnets for automotive applications. *IEEE Trans. Ind. Electron.*, **61**(10):5749-5756, [doi:10.1109/TIE.2013.2289856]

Mutoh, N., 2012. Driving and braking torque distribution methods for front- and rear-wheel-independent drive-type electric vehicles on roads with low friction coefficient. *IEEE Trans. Ind. Electron.*, **59**(10):3919-3933. [doi:10.1109/TIE.2012.2186772]

Nerg, J., Rilla, M., Ruuskanen, V., *et al.*, 2014. Direct-driven interior magnet permanent-magnet synchronous motors for a full electric sports car. *IEEE Trans. Ind. Electron.*, **61**(8):4286-4294. [doi:10.1109/TIE.2013.2248340]

Pellegrino, G., Vagati, A., Boazzo, B., *et al.*, 2012a. Comparison of induction and PM synchronous motor drives for EV application including design examples. *IEEE Trans. Ind. Appl.*, **48**(6):2322-2332. [doi:10.1109/TIA.2012.2227092]

Pellegrino, G., Vagati, A., Guglielmi, P., *et al.*, 2012b. Performance comparison between surface-mounted and interior PM motor drives for electric vehicle application. *IEEE Trans. Ind. Electron.*, *59*(2):803-811. [doi:10.1109/TIE.2011.2151825]

Phi, H.N., Hoang, E., Gabsi, M., 2011. Performance synthesis of permanent-magnet synchronous machines during the driving cycle of a hybrid electric vehicle. *IEEE Trans. Veh. Technol.*, **60**(5):1991-1998. [doi:10.1109/TVT.2011.2118776]

Reddy, P.B., El-Refaie, A.M., Huh, K.K., *et al.*, 2012. Comparison of interior and surface PM machines equipped with fractional-slot concentrated windings for hybrid traction applications. *IEEE Trans. Energy Conv.*, **27**(3):593-602. [doi:10.1109/TEC.2012.2195316]

Sizov, G.Y., Ionel, D.M., Demerdash, N.A.O., 2012. Modeling and parametric design of permanent-magnet AC machines using computationally efficient finite-element analysis. *IEEE Trans. Ind. Electron.*, **59**(6):2403-2413. [doi:10.1109/TIE.2011.2163912]

Vaez-Zadeh, S., Ghasemi, A.R., 2005. Design optimization of permanent magnet synchronous motors for high torque capability and low magnet volume. *Electr. Power Syst. Res.*, **74**(2):307-313. [doi:10.1016/j.epsr.2004.11.008]

Wang, A., Jia, Y., Soong, W.L., 2011. Comparison of five topologies for an interior permanent-magnet machine for a hybrid electric vehicle. *IEEE Trans. Magn.*, **47**(10): 3606-3609. [doi:10.1109/TMAG.2011.2157097]

Wang, D.Y., Guan, C., 2013. Optimal control for a parallel hybrid hydraulic excavator using particle swarm optimization. *Sci. World J.*, **2013**:831564.1-831564.6. [doi:10.1155/2013/831564]

Wang, T., Wang, Q.F., 2012. Optimization design of permanent magnet synchronous generator for a potential energy recovery system. *IEEE Trans. Energy Conv.*, **27**(4):856-863. [doi:10.1109/TEC.2012.2211080]

Xiao, Q., Wang, Q.F., Zhang, Y.T., 2008. Control strategies of power system in hybrid hydraulic excavator. *Autom. Constr.*, **17**(4):361-367. [doi:10.1016/j.autcon.2007.05.014]

Zhu, Z.Q., Howe, D., 2007. Electrical machines and drives for electric, hybrid, and fuel cell vehicles. *Proc. IEEE*, **95**(4):746-765. [doi:10.1109/JPROC.2006.892482]

Zhu, Z.Q., Wu, L.J., Xia, Z.P., 2010. An accurate subdomain model for magnetic field computation in slotted surface-mounted permanent-magnet machines. *IEEE Trans. Magn.*, **46**(4):1100-1115. [doi:10.1109/TMAG.2009.2038153]